Journal of Materials Research and Technology 27 (2023) 8062–8072

Contents lists available at ScienceDirect

Journal of Materials Research and Technology

journal homepage: www.elsevier.com/locate/jmrt

Comparative kinetics study of different iron-containing pellets with hydrogen at isothermal conditions

Manish Kumar Kar [a,*], Mengyi Zhu [a], Jafar Safarian [a]

[a] Department of Materials Science and Engineering, Norwegian University of Science and Technology, Alfred Getz Vei 2, 7491 Trondheim, Norway

ARTICLE INFO

Handling Editor: P Rios

Keywords:
Iron ore
Bauxite residue
Hydrogen reduction
Isothermal
Kinetics
Porosity

ABSTRACT

Using hydrogen to produce iron is a promising way for the steel industry to achieve the goal of carbon neutrality. The reducibility of iron-bearing oxides by hydrogen significantly impacts the productivity and energy consumption during the reduction process. This study investigated the competitive kinetics of hydrogen reduction for different iron bearing pellets including iron ore pellets, bauxite residue pellets, and calcium-added bauxite residue sintered and self-hardened pellets at isothermal condition. Various characterization tools, such as X-ray diffraction, electron probe analysis, and X-ray fluorescence, were used to examine the properties of the pellets. These pellets exhibit different porosity, iron bearing oxides and overall composition. The time required to achieve 50 % reduction(R_{50}) at 1000 °C approximately 2 min for bauxite residue and bauxite residue-CaO sintered and self-hardened pellets, while iron ore pellets required approximately 6 min. Moreover, at 700 °C, the R_{50} value is reduced for sintered bauxite residue CaO pellets as compared to other owing to the diminished reducibility of brownmillerite ($Ca_2(Al_x,Fe_{(2-x)})O_5$) in contrast to hematite found in the other pellets. It was highlighted that factors such as porosity of the unreduced pellets, types of iron bearing oxides and grainsize significantly influences the reducibility of different pellets. Furthermore, during the reduction process, all pellets were observed with a rapid initial stage, a subsequent transition stage, and a final slow reduction stage.

1. Introduction

As global energy demand escalates alongside pressing concerns about carbon neutrality, the world is facing an increasingly evident need for energy transition [1]. Currently, most energy consumption is derived from the combustion of fossil fuels, a primary contributor to global warming. Furthermore, significant metal reduction relies on carbon as a reductant, producing CO and CO_2 as byproducts, which significantly contribute to greenhouse gas emissions. Consequently, the dependency on fossil fuel-based energy is both unstable and environmentally detrimental, prompting the search for alternative fuels. Amidst concerns about global climate change and the need for green energy, low-carbon, emission-free fuels have become a priority. Hydrogen, as an alternative fuel, has the potential to satisfy energy demand with its high specific energy content and green reductant properties. The iron and steel industry contributes approximately 7 % of the global CO_2 emissions. Thus, the Paris agreement (COP21) requires steel mills to reduce their CO_2 emission from 3000 MT/year to below 500 MT/year, necessitating several process redevelopments [2]. The industry has already initiated the DR-EAF route for steel production using hydrogen; however, the primary challenge lies in procuring affordable hydrogen to make the process cost-competitive with conventional BF-BOF methods.

Some relevant literature pertains to the reduction behavior of iron bearing oxides and modeling work that considers pellet porosity and grain size. Ding et al. (2018) investigated the reduction behaviors of $2CaO{\cdot}Fe_2O_3$ and $CaO{\cdot}Fe_2O_3$ by hydrogen at various temperatures. Their finding indicated that the $CaO{\cdot}Fe_2O_3$ exhibited a higher reduction degree and a higher extent of reduction than $2CaO{\cdot}Fe_2O_3$. The reaction of $2CaO{\cdot}Fe_2O_3$ with H_2 is directly producing CaO and metallic iron, while the reduction of $CaO{\cdot}Fe_2O_3$ with hydrogen goes through four steps in sequence via the formation of $CaO{\cdot}FeO{\cdot}Fe_2O_3$, $CaO{\cdot}3FeO{\cdot}Fe_2O_3$, $2CaO{\cdot}Fe_2O_3$ and eventually with the generation of Fe species [3]. Furthermore, literature contains modeling-based study that highlighted the effect of porosity and reduction rate(reducibility) [4,5]. Szekely et al. (1971) investigated the structural model for the reaction of porous solid pellets with reactant gases. They highlighted that both grain size and porosity of pellets plays a significant role in diffusivities of reactant and product gases, with a focus on chemical reaction on the individual

* Corresponding author.
E-mail address: manish.k.kar@ntnu.no (M.K. Kar).

https://doi.org/10.1016/j.jmrt.2023.11.248
Received 16 September 2023; Received in revised form 11 November 2023; Accepted 26 November 2023
Available online 29 November 2023

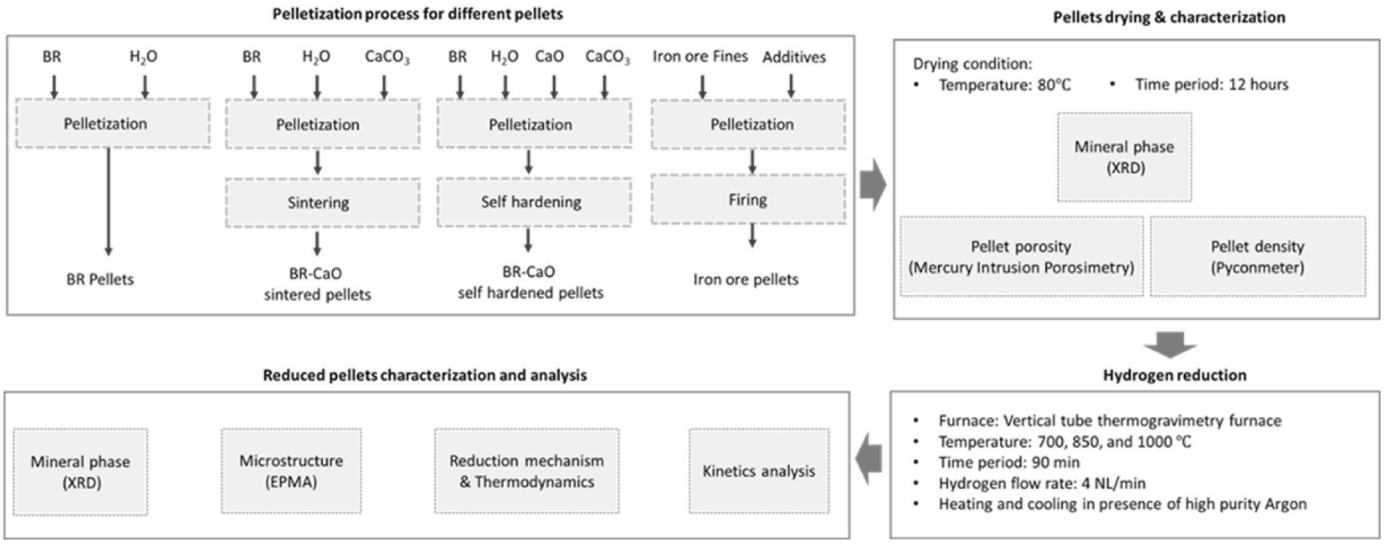

Fig. 1. Over all experimental process.

grains are important [5].

Although numerous studies have investigated the hydrogen reduction of iron ore pellets [6–9], however, there is still very limited research concerning the study of hydrogen reduction of red mud or bauxite residue (BR) pellets [10,11]. As the demand for iron keeps increasing and the quality and grade of the ore decreases, high iron content bauxite residue could serve as an important iron source if it can extract economically. Therefore, extracting the metallic value from bauxite residue is essential to reducing the waste and it can be used as iron resources for iron production. Thus, a comparative study examining the hydrogen reduction kinetics of bauxite residue versus conventional iron ore is of significant importance.

A sustainable process has been introduced by the HARARE EU project(https://h2020harare.eu/) to extract iron, alumina and REEs from BR. In this process and hydrogen reduction has been conducted to reduce iron oxide to metallic iron, followed by the magnetic separation of iron recovery. This work is a part of calcium route of the HARARE project, where both bauxite residue and calcite pellets were subjected to hydrogen reduction. The purpose of incorporating calcite into bauxite residue to create a calcium aluminate phase during hydrogen reduction, so that alumina can be recovered by alkali leaching using sodium carbonate solution. After hydrogen reduction, the bauxite residue calcite pellets underwent a magnetic separation process to recover iron. The non-magnetic portion was then subjected to an alkali leaching process to recover alumina. Following the leaching process, the residue became enriched with calcite and rare earth elements. This enriched calcite residue was subsequently recycled to produce bauxite residue calcite pellets, completing a sustainable materials loop within the process [12,13].

In this work, we studied the relationship between hydrogen reduction behavior of different BR pellets and conventional iron ore pellets with respects to pellets porosity and iron oxides complexes. Through the experimental work, a comparative kinetics study of hydrogen reduction behaviors of various pellet types, including BR pellets, sintered BR-CaO pellets, self-hardened BR-CaO pellets, and industrial iron ore pellets were conducted. Moreover, aiming to demonstrate the relationship between the reduction behaviors and the premeasured porosity of these pellets, a combination of analytical techniques such as X-ray fluorescence (XRF) for chemical analysis, scanning electron probe micro analyzer (EPMA) for microstructural examination, X-ray diffraction (XRD) were employed for phase analysis and mercury intrusion porosimeter for porosity and to provide a comprehensive understanding of the hydrogen reduction behaviors of the various pellet types.

2. Materials and methods

2.1. Experimental methodology

The complete experimental methodology is described in Fig. 1.

2.1.1. Agglomeration of pellets

BR, limestone, and quick lime were utilized as raw materials for BR agglomerated pellets. BR was supplied by Mytilineous Business Unit S. A., Greece (previously known as aluminum of Greece), limestone from VUGIUKLI S.A., Greece, and quick lime was from the NorFraKalk. The raw materials were received in lumpy form, and then deagglomerated below 500 μm sieve size, and dried in an oven for 24 h at 80 °C. After the drying process, these materials were mixed in a lab mixer with appropriate composition based on the pellet types. The CaO were added with calculated fractions to form compounds of $CaO{\cdot}Al_2O_3$, $2CaO{\cdot}SiO_2$ and $CaO{\cdot}TiO_2$ in different BR-lime pellets as outlined previously [14]. However, the BR to calcium oxide ratio for sintered BR-CaO pellet and self-hardened BR-CaO pellets were fixed despite of different chemical compositions of raw materials. Mixed materials were pelletized in the drum pelletizer via 10 wt% water addition. The average size range is about 8–10 mm for all different pellets.

The sintered BR-CaO pellets were produced by drying BR-$CaCO_3$ green pellets overnight in an oven and then sintered at 1150 ± 10 °C for 120 min in a muffle furnace [14]. Self-hardened pellets were made by mixing the BR with CaO and $CaCO_3$ with appropriate composition [15]. The green pellets were aged in air (room temperature) for three days to increase the pellet strength. The mechanism of self-hardening of pellets was presented in our previous study [15]. The commercial iron ore pellets were from the ferrous industry.

2.1.2. Hydrogen reduction in Thermogravimetry (TG) furnace

The reduction experiments were carried out in a TG furnace, which comprised a vertical tube furnace, stainless steel hollow cylindrical crucible, a gas flow controller, an electronic balance, and a temperature controller. The schematic view of the furnace and the working principle were described in our previous paper [15]. These pellets were heated in the presence of argon with a flow of 1NL/min up to the targeted temperature 1000 ± 10 °C. The heating rate was maintained at 10 °C/min to homogenize temperature inside the pellet bed. The temperature of the sample bed was measured using a thermocouple inserted inside the sample bed. For self-hardened BR-CaO pellets, there was no remaining calcite (all converted to CaO) when the set point temperature reached.

Table 1
Mass loss(wt.%) due to hydrogen reduction of different pellets at different temperatures.

Pellets/ Temperature (°C)	BR pellets	Self-hardened pellets	Sintered pellets	Iron ore pellets
1000	14.36	9.36	11.52	28.72
850	13.92	7.90	10.88	28.60
700	8.57	5.28	6.72	28.15

This was confirmed by the absence of mass loss observations. Hence, after getting stable weight at the targeted temperature, H_2 gas was purged with a flow rate of 4NL/min for 90 min. After the reduction time was over, sample cooling was carried out in presence of argon (flow rate 1NL/min) to avoid reoxidation of reduced iron. These conditions were the same for all types of pellets. To cross-check the actual weight loss and the weight loss recorded by the data logger, weight loss measurements were taken by sample mass weighting before and after the process.

2.2. Characterization of materials

The mineralogical phases in the samples were identified using XRD analysis with Bruker D8 focus (Bruker AXS GmbH, Karlsruhe, Germany) and CuKα radiation($\lambda = 1.54$ Å) with a scan speed of 0.03°. After obtaining XRD pattens, the phases were identified using EVA software by diffraction database. For the XRD sample preparation, pellets were milled by a WC vibratory disk mill (RS200, RETSCH GmbH, Haan, Germany) for 60 s at 900 revolution per minute (rpm). In addition, chemical composition analysis and X-ray mapping were obtained by using X-ray fluorescence and electron probe micro analyzer (EPMA) (JXA-8500F.JEOL Ltd., Akishima, Japan) respectively. The porosity of the pellets was evaluated utilizing mercury intrusion porosimeter (Autopore IV 9520, Micromeritics, USA). Pressurized mercury was employed to fill void space inside the pellets and porosity was calculated. Furthermore, the density of the pellets were determined by a pycnometer (Micromeritics, Accupyc 1340, USA) with helium gas injection.

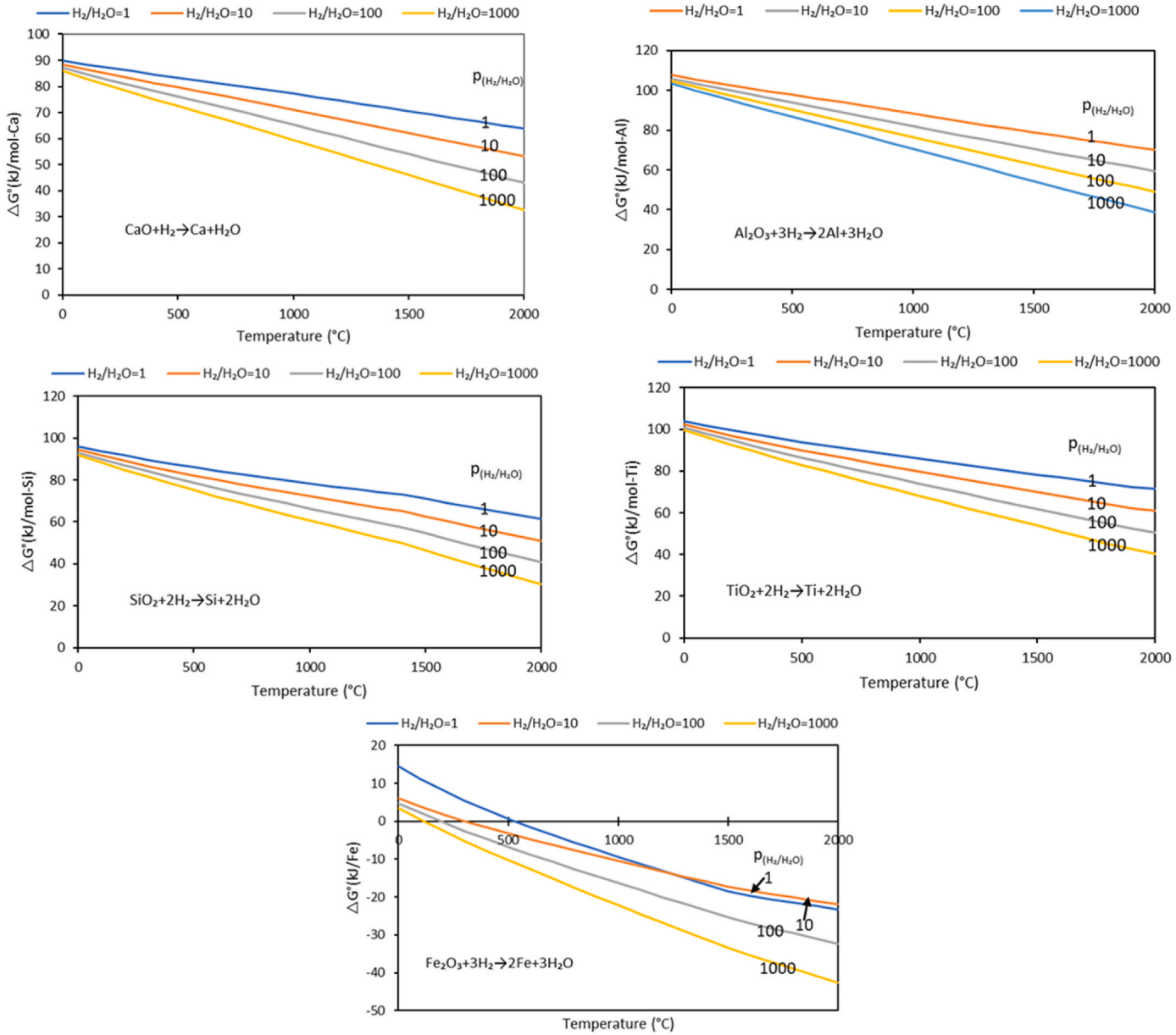

Fig. 2. Standard free energy of reduction with H_2 at different $\frac{p_{H_2}}{p_{H_2O}}$ ratios for (1) CaO (2) Al_2O_3 (3) SiO_2 (4) TiO_2 (5) Fe_2O_3.

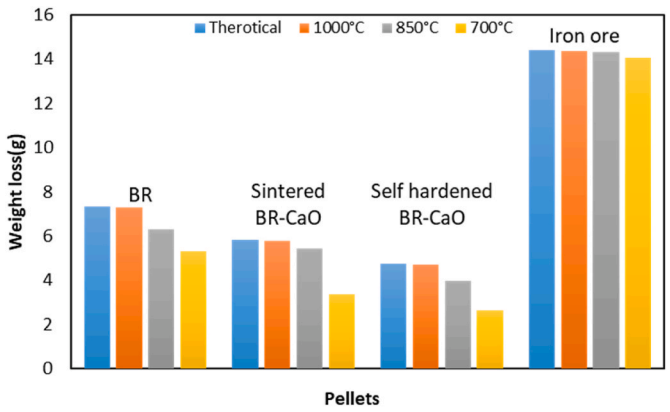

Fig. 3. Weight loss is measured with initial mass of 50 g for different pellets.

3. Results and discussion

3.1. Mass losses during reduction

The mass loss results of pellets at varying reduction temperatures are presented in Table 1. There is minimal difference between mass losses for BR, self-hardened BR-CaO and sintered BR-CaO pellets reduced at 850 °C and 1000 °C temperature. However, the mass losses at 700 °C reduction was much less for BR, Sintered BR- CaO, and self-hardened BR-CaO pellets, which may be due to the slower reduction kinetics. In the case of iron ore pellets, the weight reduction is almost similar for the three temperatures, which may be due to complete direct reduction of hematite to iron.

At a reduction temperature of 1000 °C, the mass loss of all pellets is nearly equal to the theoretical mass losses. The theoretical mass losses were calculated based on the oxygen present in iron oxide in the pellets. The calculated theoretical mass losses and weight loss during reduction for different pellets are presented in Fig. 3. As major fraction of oxides present in sample are Al_2O_3, SiO_2, TiO_2, CaO and Fe_2O_3, and at the operated reduction temperature in the presence of hydrogen, only iron can be reduced as other oxides are much stable at that reduction temperature. When there is a consistent flow of hydrogen gas into the

Table 2
XRF analysis of reduced pellets (wt.%).

Oxides/Pellets	Al_2O_3	CaO	Fe	K_2O	MnO	MgO	Na_2O	P_2O_5	SO_3	SiO_2	TiO_2	Cr_2O_3	V_2O_5	NiO	LOI
Sinter BR-CaO	23.60	35.90	21.40	0.09	0.05	0.87	2.22	0.10	0.86	9.75	4.39	0.20	0.13	0.06	0.24
BR	26.32	11.89	37.62	0.11	0.08	0.36	4.08	0.10	0.89	10.24	7.34	0.38	–	0.13	NA
Self-hardened BR-CaO	19.15	40.19	23.04	0.05	0.04	0.49	2.57	0.09	0.84	7.32	5.02	0.23	–	0.08	5.8
Iron ore	0.82	0.87	88.1	0.1	0.08	1.66	0.42	0.07	–	7.47	0.2	0.01	0.15	0.03	0.01

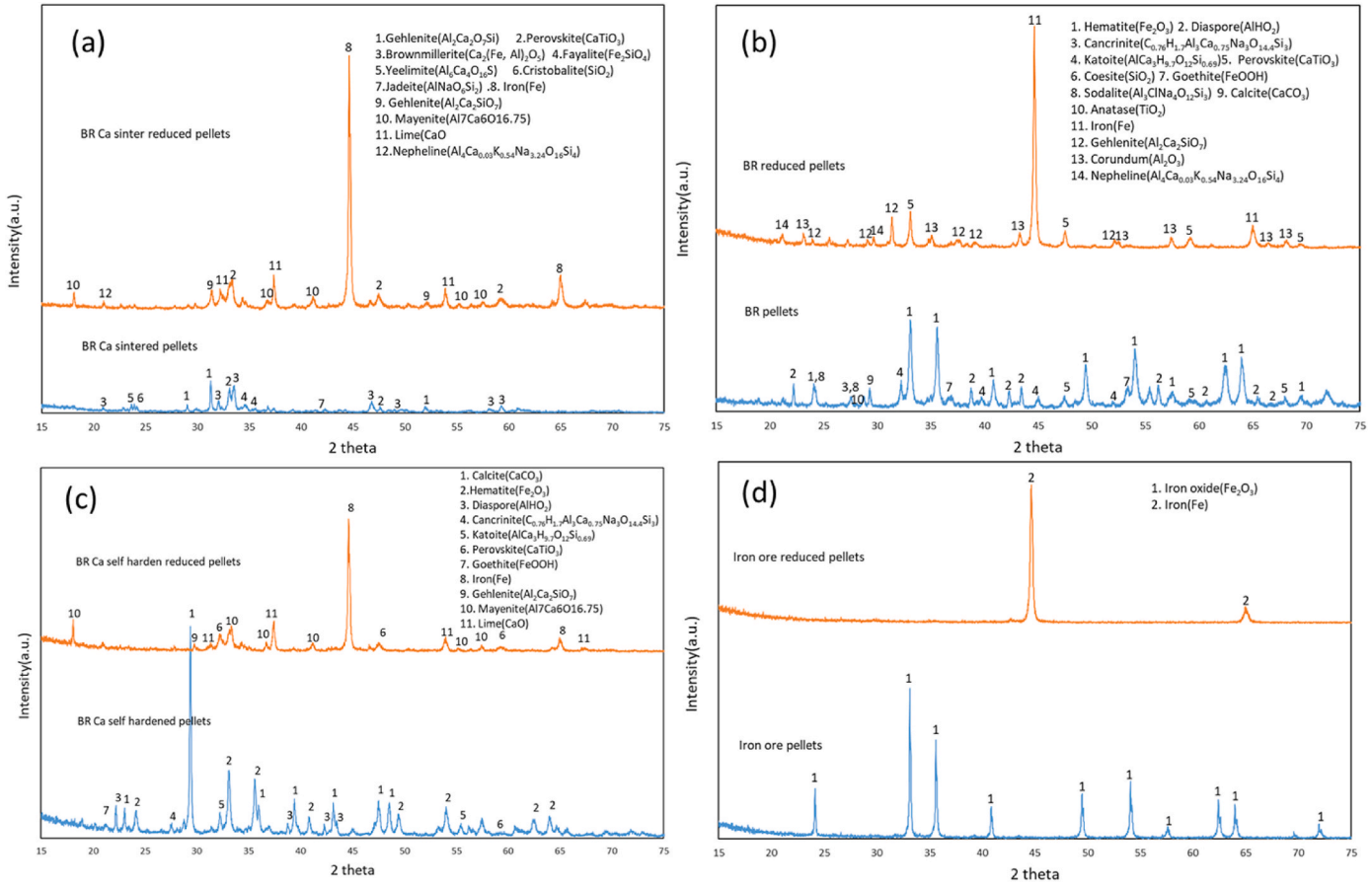

Fig. 4. Phase analysis of the raw materials and reduced pellets at 1000 °C, (a)Sintered BR CaO pellets (b)BR pellets (c)Self hardened BR CaO pellets (d)Iron ore pellet.

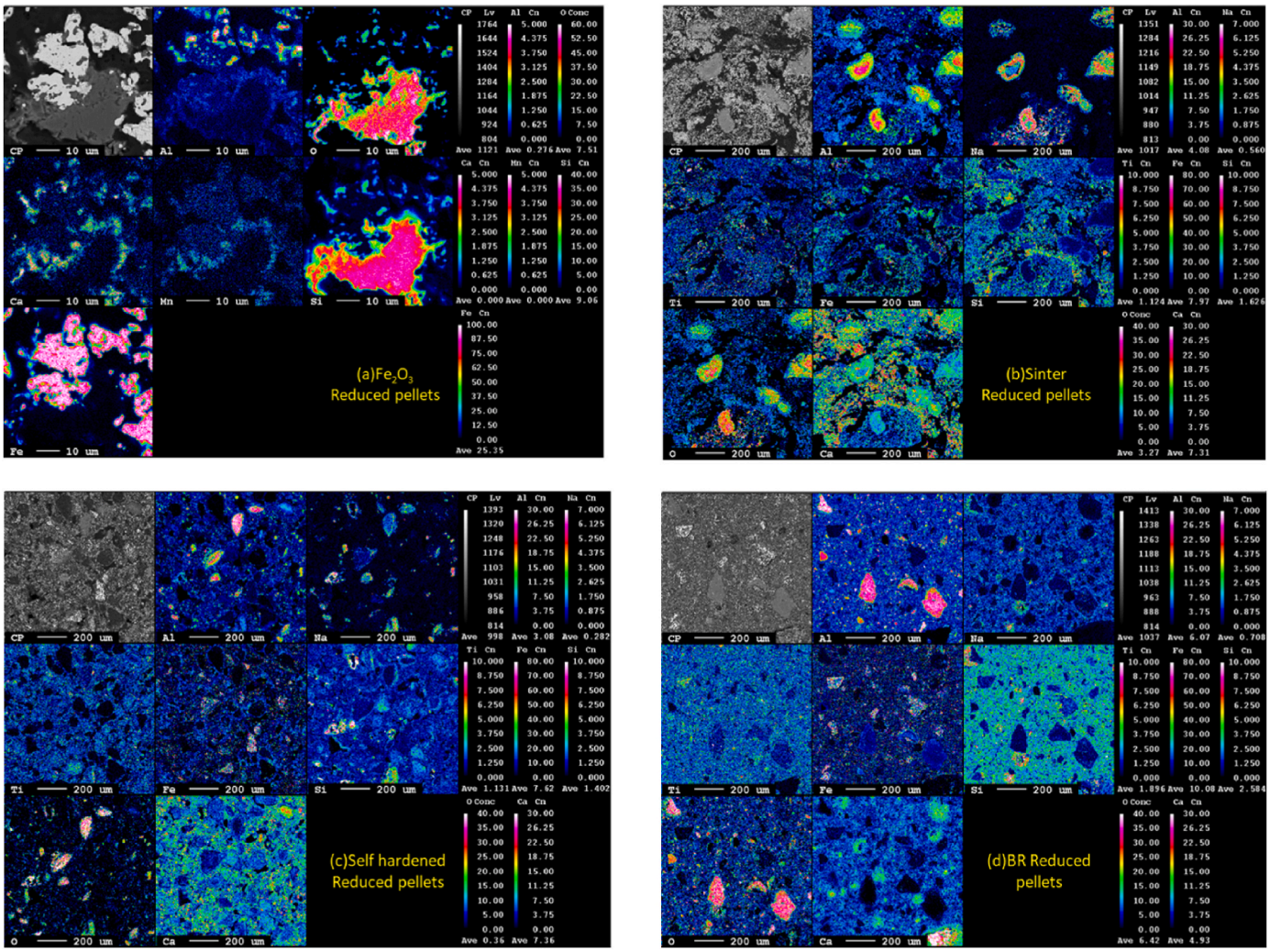

Fig. 5. EPMA elemental mapping of iron ore pellets(a), Sinter BR CaO pellets(b), Self-harden BR CaO pellets(c), BR pellets (d) reduced at 1000 °C.

sample bed, the real partial pressure $\frac{p_{H_2}}{p_{H_2O}}$ is significantly higher than the corresponding ratio at equilibrium. With increases in $\frac{p_{H_2}}{p_{H_2O}}$ ratio the reduction reaction starts at lower temperature. Yet, even with increasing $\frac{p_{H_2}}{p_{H_2O}}$, all the other oxides, apart from iron oxide, still have the positive free energy of reduction except iron oxide, shown in Fig. 2. Thus, suggests that only Fe_2O_3 underwent reduction in the sample at the applied temperatures.

3.2. Properties of reduced pellets

3.2.1. Chemical analysis of reduced pellets

The results of the chemical analysis of the reduced pellets are presented in Table 2. Reduced iron ore predominantly consists of metallic iron and silica as a minor fraction. Meanwhile, BR reduced pellets comprise major components such as iron, alumina, CaO, Na_2O and TiO_2. The metallic Fe in the samples and the other oxides were normalized with regard to the XRD analysis data (see section 3.2.2.) of the samples, and in Table 2 they were presented in the form of most simple/stable oxides. Although a small quantity of unreduced iron in the form of FeO was anticipated, the XRD data did not indicate its presence, confirming that all iron is in the reduced state.

3.2.2. Phase analysis

Phase analysis of the raw materials and reduced pellets (Reduction temperature 1000 °C) were carried out by XRD, and the results are presented in Fig. 4. As seen in Fig. 4(d), the iron in the iron ore pellets present majorly in form of Fe_2O_3, whereas in the reduced pellets only metallic iron was identified. This indicates that most of the Fe_2O_3 is reduced to metallic iron. The conclusion is also correlated with microstructural analysis (Fig. 5(a)). As shown in Tables 2 and in the reduced iron ore pellets, a minor quantity of SiO_2 is present. However, it was not detected in the XRD analysis, possibly owing to its minor fraction. It may also be possible that it has amorphous form in pure or combination with the gangue (CaO, MgO), and not detected by XRD [16]. In the BR and BR-CaO reduced pellets, metallic iron(Fe), perovskite ($CaTiO_3$), gehlenite ($Ca_2Al_2SiO_7$), corundum (Al_2O_3), nepheline ($Al_4Ca_{0.03}K_{0.54}Na_{3.24}O_{16}Si_4$), mayenite ($Al_7Ca_6O_{16.75}$) and lime (CaO) are the major phases. Similar to iron ore pellets, in BR reduced pellets, all iron oxide was reduced to metallic iron. Aluminum is present in BR and BR-CaO oxide pellets as gehlenite, corundum and nepheline phases, while titanium present in the form of perovskite. In the reduced sinter BR-CaO and the reduced self-harden BR-CaO pellets, all the phases are similar with varying intensities. When BR CaO(self-hardened) pellets are reduced, the added calcium oxide reacts with alumina present in BR at elevated temperatures to form mayenite. The mayenite phase was not present in BR reduced pellets due to the low CaO content and its favor to react with TiO_2 to form perovskite. In the case of sintered BR-CaO pellets, the added CaO to BR causes Al_2O_3 converted to gehlenite and nepheline phases during the sintering step and remaining aluminum stays as unreacted corundum phase. For all the pellets reduced at

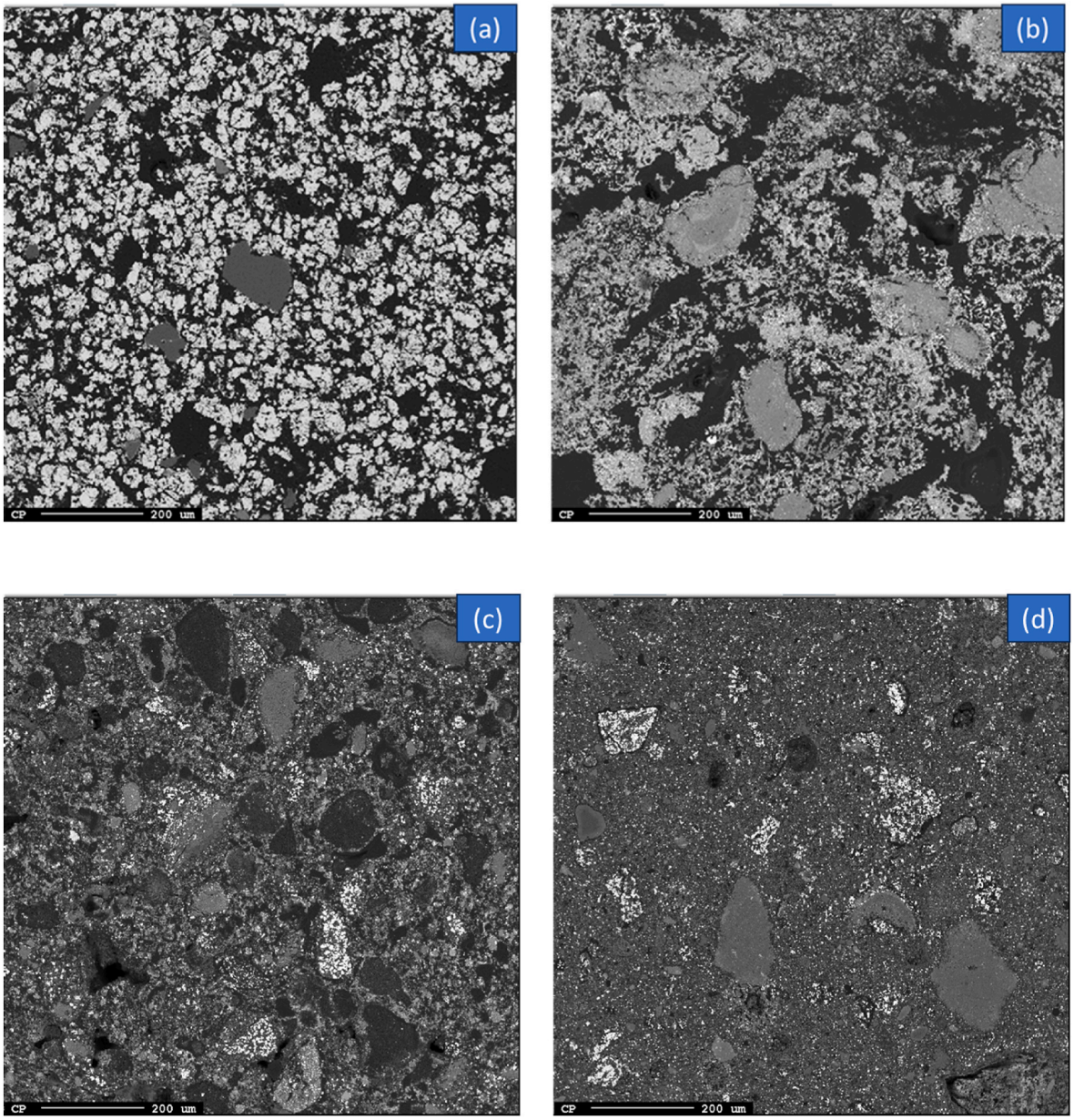

Fig. 6. SEM images of reduced iron ore pellets(a), reduced sintered BR-CaO pellet(b), reduced self-hardened BR-CaO pellets (c), reduced BR pellets (d) at 1000 °C.

1000 °C, the iron complexes (hematite, goethite, brownmillerite, srebrodolskite and fayalite) were converted to metallic iron after reduction and no unreduced iron oxides were detected.

In the iron ore pellets, iron oxide completely reduced at 850 °C and 700 °C to metallic iron with some silica peak was observed. In the BR and self-hardened BR-CaO pellets reduced at 850 °C, majority of all iron oxide is reduced. However, at 700 °C, it was converted to a mixture of metallic iron, magnetite and minor brownmillerite. Along with iron, calcium oxide, perovskite, gehlenite phases are found in 850 °C and 700 °C reduced pellets. As for the sintered BR-CaO pellets reduced at 850 °C and 700 °C temperatures, iron present in from of brownmillerite and metallic iron. The spectrum of metallic iron is more intense for pellets reduced at 850 °C temperature as compared to 700 °C.

3.2.3. *Microstructural analysis*

Fig. 5(a) to 5(d) represent the elemental mapping of the reduced iron ore, reduced BR, reduced sinter BR-CaO and reduced self-harden BR-CaO pellets, respectively. The back scattered image of reduced iron ore pellets is present in Fig. 5(a) in which the image magnifies an area with high silica. In the elemental mapping of reduced iron ore pellets, inside metallic iron there is very little oxygen still present, nevertheless, this was not detected in the XRD analysis which may be due to background noise. In the reduced sinter BR-CaO pellets, the produced metallic iron is dispersed throughout the oxide matrix (Fig. 5(b)). In certain areas, there is an overlap of Ca and Ti with O, indicating the presence of the $CaTiO_3$ phase. Meanwhile, the Ca, Al and O overlap in some other areas with small fraction of Na, which signifies the mayenite phase. It worth noting that all the phases found in the elemental and microstructural analysis are well correlated with the identified XRD phases. The elemental analysis of the reduced sinter BR-CaO pellets (Fig. 5(b)) and reduced self-harden BR-CaO pellets (Fig. 5(c)) are showing the same microstructure, except that in the sintered sample, the intensity of Al, Ca, O and Si in some areas are more intense. The more intense area is due to the gehlenite in the sintered reduced pellets as compared self-hardened reduced pellets. In fact, during the sintering of dry pellets, more gehlenite phase was formed, which remains stable even during reduction or its reduction requires longer period.

In the reduced BR pellets, metallic iron is distributed uniformly

Table 3
Physical properties of the raw pellets.

Properties/ Pellets	BR dry pellets	Self-hardened BR CaO Pellets	Sintered BR CaO pellets	Iron ore pellets
Porosity	61.01	57.21	54.99	29.55
Density	3.15	3.10	3.51	5.09
Intrusion volume	0.41	0.4	0.33	0.07
Mean pore diameter	0.57	0.07	0.087	0.03
Total pore area	33.46	29.39	15.37	9.74

without overlapping of O, represents the complete reduction of iron oxide (calcium ferrite) to metallic iron. In certain areas, Al is associated with O as corundum phase, as present in Fig. 5(d). Notably, no overlapping of Ca, Al and O elements was observed which confirms the absence of mayenite phase in the BR reduced pellets.

The iron ore pellets underwent almost complete reduction of iron oxide during the process, which results in formation of metallic iron with particle size above 20 μm. The metallic iron is the matrix with SiO_2 phase between the iron particles, along with some fraction of CaO and MnO. With in the metallic iron matrix, the presence of minor silica particle can be observed, as seen in Fig. 6(a). In both reduced self-harden BR-CaO pellets and reduce BR pellets (Fig. 6(c) and d), metallic iron present in form of clustered fine particles. However, the reduced sinter BR-CaO pellets (Fig. 6(b)) feature smaller and ubiquitously distributed metallic iron particles. The matrix of the reduced sinter BR-CaO pellets are more compacted due to significant sintering as compared to the reduced self-harden BR-CaO pellets and reduced BR pellets. Hence, for the sintered BR-CaO pellets, the reduction occurs on a more homogeneously distributed brownmillerite phase all the entire sample, and its reduction yield finer iron particles with less clustering compared to the other two BR pellets.

3.2.4. *Physical properties of the unreduced pellets*

During the gas-solid reaction, the interfacial area between the solid and gas phase is of vital importance. A larger interfacial area of the pellets increases the contact area between the reactant gases and solid, consequently promoting the interfacial reaction rate. Thus, a greater porosity results in more interfacial area and faster reaction rate. Results

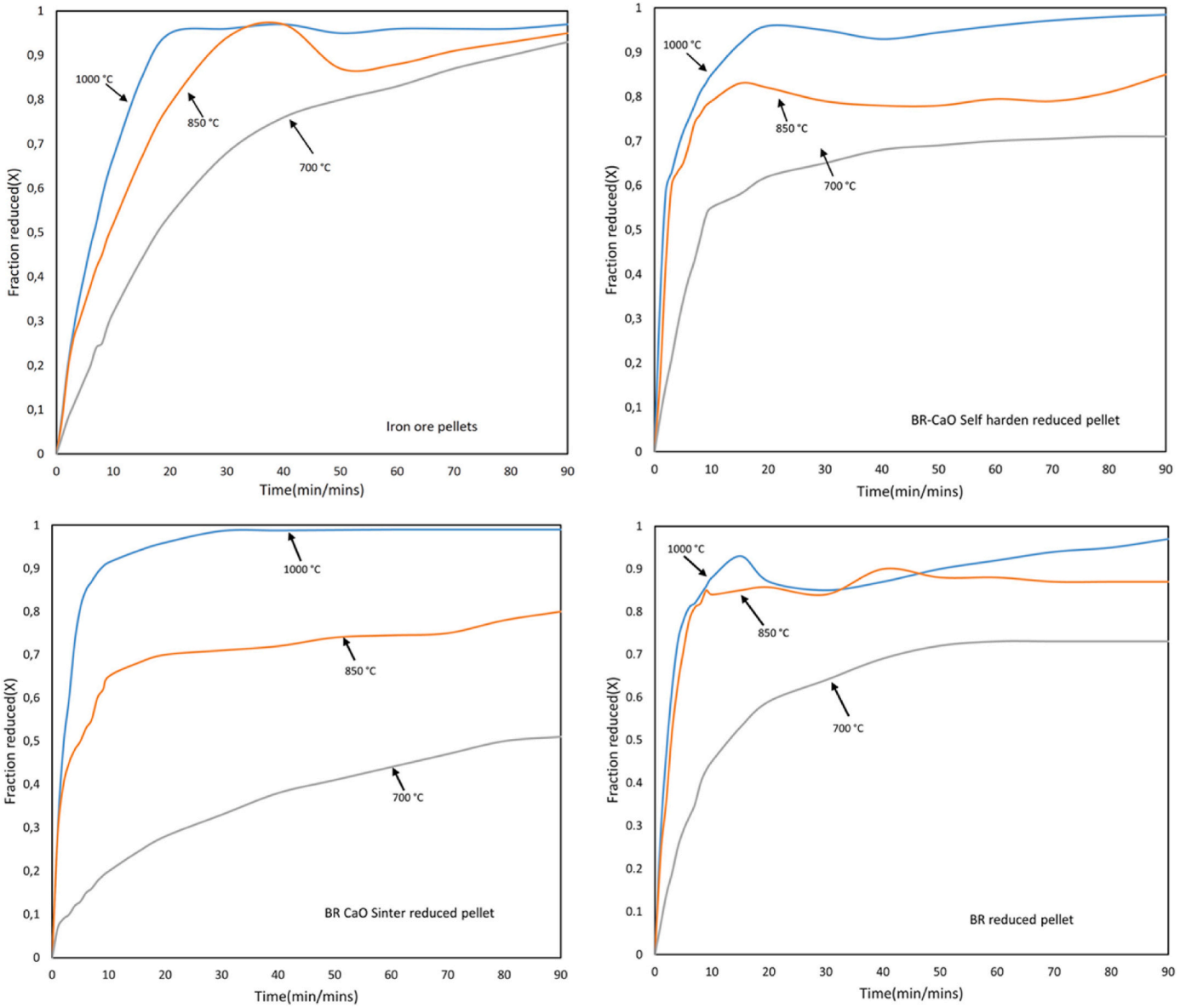

Fig. 7. Fraction of oxides reduced versus time in different pellets at different temperatures.

Table 4
Time for 50 % reduction at different temperatures for different pellets.

Pellets/Temperature (°C)	BR	Sinter BR CaO	Self-hardened BR CaO	Iron ore
1000 (°C)	2	2.1	1.8	6.5
850 (°C)	2.91	2.1	2.41	9.5
700 (°C)	12.31	78.81	38	18

of the porosity, density, intrusion volume, mean pore diameter and total pore area of unreduced pellets are presented in Table 3.

The porosity of BR and BR-CaO pellets are above 50 vol%, whereas the sintered iron ore pellets exhibit a porosity of approximately 30 vol%. The lower porosity in the pellets may be attributed to high temperature sintering. However, the sintered BR-CaO pellets have more than 50 vol% porosity even after sintering, which is due to the calcite decomposition that enhances of porosity of the pellets. Since dry BR pellets were utilized in this work, the heating cycle to the targeted temperate also promoted the composition of the diaspore, goethite, gibbsite, compounds that facilitate increased porosity during reduction. For the self-hardened BR-CaO pellets, the calcite decomposition rise during the heating process improves the porosity to above 57 vol%. Both the intrusion volume and intrinsic pore diameter are greater in the BR and BR calcite pellets, which are one order larger than iron ore pellets. As shown in Table 3, with increasing porosity level, the total pore area also increases and the density decreases. Since a greater porosity promotes more reduction in a gas-solid reaction through facilitating more and faster gas molecules diffusion, it is expected that pellets with superior porosities will exhibit better reduction and increased reducibility [17].

3.3. Kinetics of hydrogen reduction of pellets

3.3.1. Fraction conversion rate

The fraction of iron oxides reduced with respect to time at different reduction temperatures are presented in Fig. 7. The fraction reduced (X) was calculated based on the following equation.

$$X = \frac{(\Delta w)}{(w_{in})} \tag{1}$$

where $\triangle w$ is the weight loss during reduction time t, w_{in} represents the mass of oxygen present in the Fe_2O_3 in initial mass of sample. The half of the reduction (R_{50}) for all the different pellets with different reduction temperature are presented Table 4. The half of reduction was reached for BR and BR-calcite pellets (sintered and self-hardened) in about 2 min of reduction at 1000 °C, however, for the Fe_2O_3 pellets, the half of reaction was after 6.5 min at this temperature. Similar reduction rate was observed for all pellets reduced at 850 °C. The lower rate of reduction of iron ore pellets compared to BR and BR-calcium pellets may owing to the lower porosity of this pellet. As listed in Table 3, the porosity of BR and BR-calcite pellets is near about twice than iron ore pellets. However, the half of reduction completion is different for pellets reduced at 700 °C. The halftime of reduction for sintered BR-CaO pellets was longer compared to other three pellets. As from the previous work, the iron present in the sintered pellets is in the form of brownmillerite [15]. The reduction of brownmillerite with hydrogen is thermodynamically feasible near 1000 °C as per thermodynamics calculation, and its reducibility is obviously lower at lower temperatures regarding the curves in Fig. 9, along with the detection of Fe in all reduced samples of this pellet. However, for iron ore, BR and self-hardened BR CaO pellets, major fraction of iron present in form of hematite, and the reduction of hematite with hydrogen is feasible at lower temperatures with a higher rate as seen in Fig. 9 than brownmillerite. At 1000 °C, both BR and BR-CaO pellets (sintered and self-hardened) exhibited a substantial reduction, with over 80 % of the fraction reduced within 5 min of reduction, but for the iron ore pellets, it took above 10 min. This may be more due to the higher porosity of the BR-containing pellets and applying high temperature wherein brownmillerite is reduced as fast as hematite at this temperature. The close reduction rate between the two phases can be observed for the two CaO-added BR pellets at 1000 °C, while the main difference is the form of iron oxide.

The hydrogen reduction process can be divided into three different regimes based on different reduction rate: initially, the reduction began with a rapid rate, and then transitioned into an intermediate transition stage, and finally settled into a slow reduction rate. In the transition stage, the process may be mixed-controlled mechanism. In the BR pellets reduced at 1000 °C and 850 °C, the reduction happened in three regimes nonetheless the transition regime is smaller.

In the early stages, the rapid rate of reduction is primarily attributed to the substantial porosity, resulting in a significant reduction extent accounting for 80–90 % of the initial reduction extent. Nevertheless, as the reduction process progresses, the rate slows down. Particularly, for BR pellets reduced at 700 °C, a notable extended transitional phase is observed follows the initial reduction extent to only approximately 50 %.

Initially, the reaction is chemical reaction rate controlled may be due to lower reduction temperature and then mixed controlled, and eventually become diffusion controlled in the final stage. The same reduction regime was observed for self-hardened BR CaO pellets as this pellet has similar Fe-bearing oxide (hematite) with the same size, and also porosity as listed in Table 3.

In the sintered BR CaO pellets, the three reduction stages occurred at different temperatures. Notably, the extent of transition stage at 700 °C is the largest, while it is the smallest at 1000 °C. Moreover, the rapid initial stage contributed to the most extensive reduction at 1000 °C ($X > 0.9$), but the smallest at 700 °C ($X < 0.1$). In the sintered BR-CaO pellets, the porosity is the same as BR pellets and self-hardened BR CaO pellets, however, the iron is present in form of brownmillerite in the sintered pellets. The reduction of brownmillerite with hydrogen is feasible at higher temperature 1000 °C based on the negative Gibbs free energies shown in Fig. 9. The mechanism is further discussed in section 3.3.3. Obviously, the reduction rate of brownmillerite is lower than hematite at lower temperatures than 850 °C. All types of BR pellets, including sintered BR CaO pellets and self-hardened BR CaO pellets, possess porosities above 50 vol%. The rate of reduction can also be influenced by several factors: the finer particle size, reducibility of brownmillerite and hematite, and the reduction temperature. Notably, the reduction temperature plays a dual role, governing both diffusion of reactant and product gases through the product layer and influencing the reducibility of the iron bearing oxides. In iron ore pellets, the initial reduction rate is slower at 1000 °C as compared to BR and BR-calcium pellets (self-hardened BR CaO), which may be due to lower porosity of the iron ore pellets and the bigger hematite particle size. It is worth noting that in all these three pellets, hematite particles were reduced by hydrogen. After 20 min of reduction, the rate became much slower may be due to diffusion of product as well as reactant gases through a thicker intermediate FeO layer (between Fe and Fe_2O_3), and according to literature, diffusion through FeO is the rate controlling step [18].

3.3.2. Reduction velocity index

Reduction velocity index (RVI) can be used to evaluate the reduction behavior of pellet. A higher RVI value is indicative of superior reducibility of the pellets. The RVI value for different pellets was calculated by equations (2) and (3) based on ISO 4695:2007(E). The standard is applicable to various iron raw materials, including lump ores, sinters and hot-bonded pellets, and sintered also contained $Ca_2Fe_2O_5$ [19], which is similar to iron complex present in sintered BR- CaO pellets.

$$\frac{dR}{dt}\left(\frac{O}{Fe} = 0.9\right) = \frac{33.6}{t_{60} - t_{30}} \text{ (Reduction above 60\%)} \tag{2}$$

$$\frac{dR}{dt}\left(\frac{O}{Fe} = 0.9\right) = \frac{26.5}{t_{y} - t_{30}} \text{ (Reduction below 50\% < y < 60\%)} \tag{3}$$

Table 5
Calculated reduction velocity index values for the reduction of different pellets.

RVI/Temp.	BR	Sinter BR CaO	Self-hardened BR CaO	Iron ore
1000 °C	18.66	16.8	17.68	6.72
850 °C	14	4.94	16.8	3.86
700 °C	6.72	0.35	2.68	2.38

where, t_{60} *and* t_{30} are the time required for degrees of reduction 30 % and 60 %, respectively, and 33.6 is a constant. t_y is the time required for degrees of reduction below 60 % and above 50 % where 26.5 is the constant. The rate of reduction in atomic scale of O/Fe = 0.9 with unit of reducibility is %/mins.

As shown in Table 5, at 1000 °C BR has the highest RVI, which is three times greater than for iron ore pellets. However, BR and BR-CaO pellets are with close RVIs, possibly due to their comparable porosities. At 850 °C, the RVI-values of BR and self-hardened BR-CaO pellets remain similar, which can be attributed to similar porosities and the existence of Fe_2O_3 as the Fe-bearing compound in them. The RVI for sintered BR-CaO pellets remain lower at 700 and 850 °C even with higher porosity of the unreduced pellets. This may again confirm the crucial role played by the type of reducible oxide involved. In the BR-CaO sintered pellets, iron is present in the form of brownmillerite, which requires higher reduction temperature for faster conversion to metallic iron. Contrastingly, the iron ore pellets exhibit a lower RVI value in comparison to both BR and BR-CaO self-hardened pellets at all three-reduction temperature, this is due to the iron present in these pellets being in the form of hematite. The lower RVI for the hematite pellet is attributed to both lower porosity and the size of hematite grains. As presented in Fig. 6, the hematite particles in the iron ore pellet are significantly larger than those in the BR pellets. Consequently, the change from the fast initial reduction stage to the second transition stage occurs at a lesser conversion rate when compared to the two other hematite containing pellets as seen in Fig. 7. Moreover, the final reduction stage is slower for the iron ore pellet as there is thicker product layer on the hematite particles of this pellet than those in the BR containing pellets due to the initial larger iron oxide particles. The schematic illustration of iron ore reduction and BR/BR CaO (sintered and self-hardened) pellets reduced at 1000 °C is presented in Fig. 8. At time t_1, the product layer thickness is identical for both the types of pellets ($L_1^S = L_1^B$), and for time t_2, the thickness is ($L_2^S = L_2^B$). At t_2 time, the BR/BR CaO pellets were completely reduced above 95 % fraction reduction. In contrast, the iron ore pellets achieved a reduction slightly below 90 %, indicating the presence of an unreduced oxide core within the pellets.

3.3.3. *Reducibility of iron bearing oxides*

The overall reduction reactions of hematite and brownmillerite with hydrogen are presented in reactions (4) and (5):

$$Fe_2O_3(s) + H_2(g) \rightarrow 2Fe(s) + 3H_2O(g) \quad (4)$$

$$7Ca_2[Fe_x, Al_{1-x}]_2O_5(s) + 21x\,H_2(g) = 14x\,Fe(s) + 21xH_2O(g) + (2+12x)CaO(s) + (1-x)Ca_{12}Al_{14}O_{33(s)} \quad (5)$$

As shown in Fig. 9, the free energy of brownmillerite reduction is positive at 1000 °C when the partial pressure of $H_2/H_2O = 1$. However, during experiments utilizing pure H_2 gas, the p_{H_2/H_2O} is much higher than the equilibrium composition. Moreover, the reduction of brownmillerite with H_2 was calculated with the activity 1, but in actual practice the activity of the products phases is less than 1. Therefore, the high partial pressure of hydrogen and the low activities of products drive the reduction reaction to the right. Consequently, even at lower reduction temperatures, the brownmillerite reduction occurs with the formation of metallic iron, albeit at slower reduction rate. In contrast, hematite presents a negative free energy of reduction across all three-reduction temperatures (1000, 850 and 700 °C) when the partial

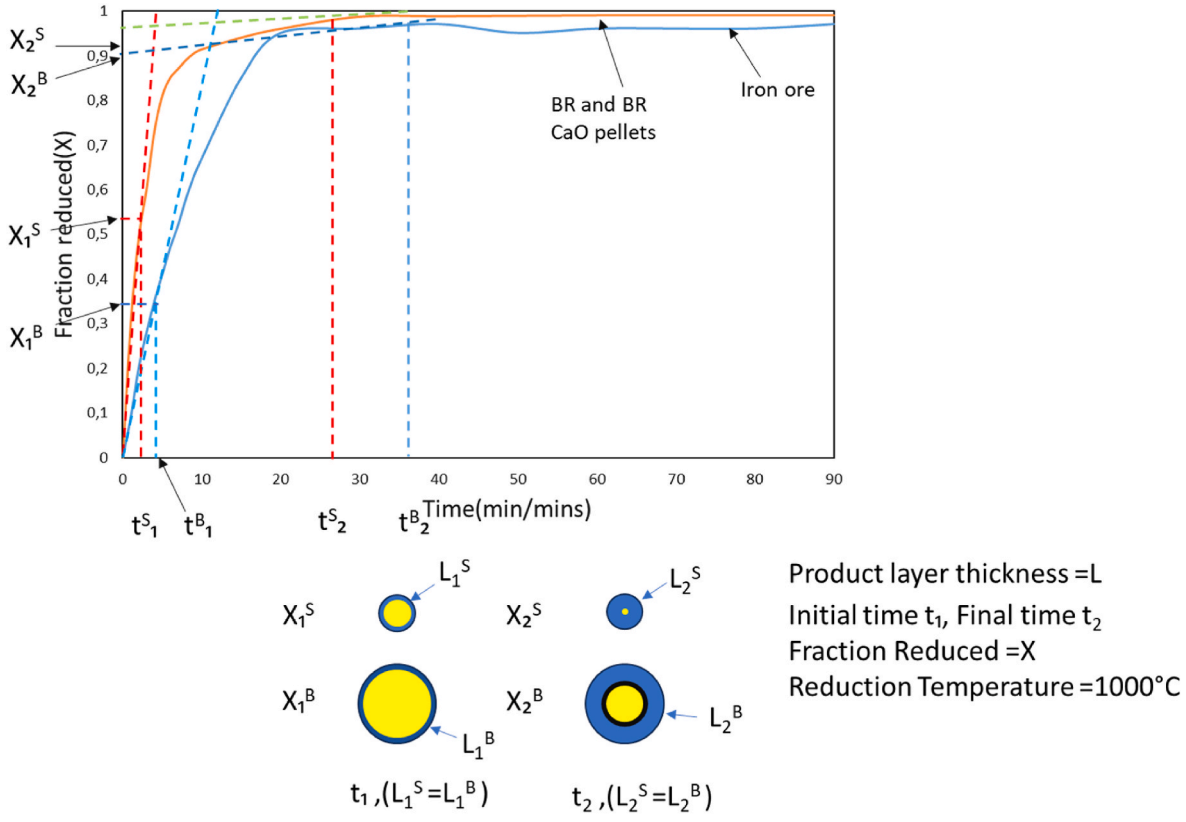

Fig. 8. Schematic illustration of reduction behavior of iron ore and BR containing pellets at 1000 °C reduction temperature.

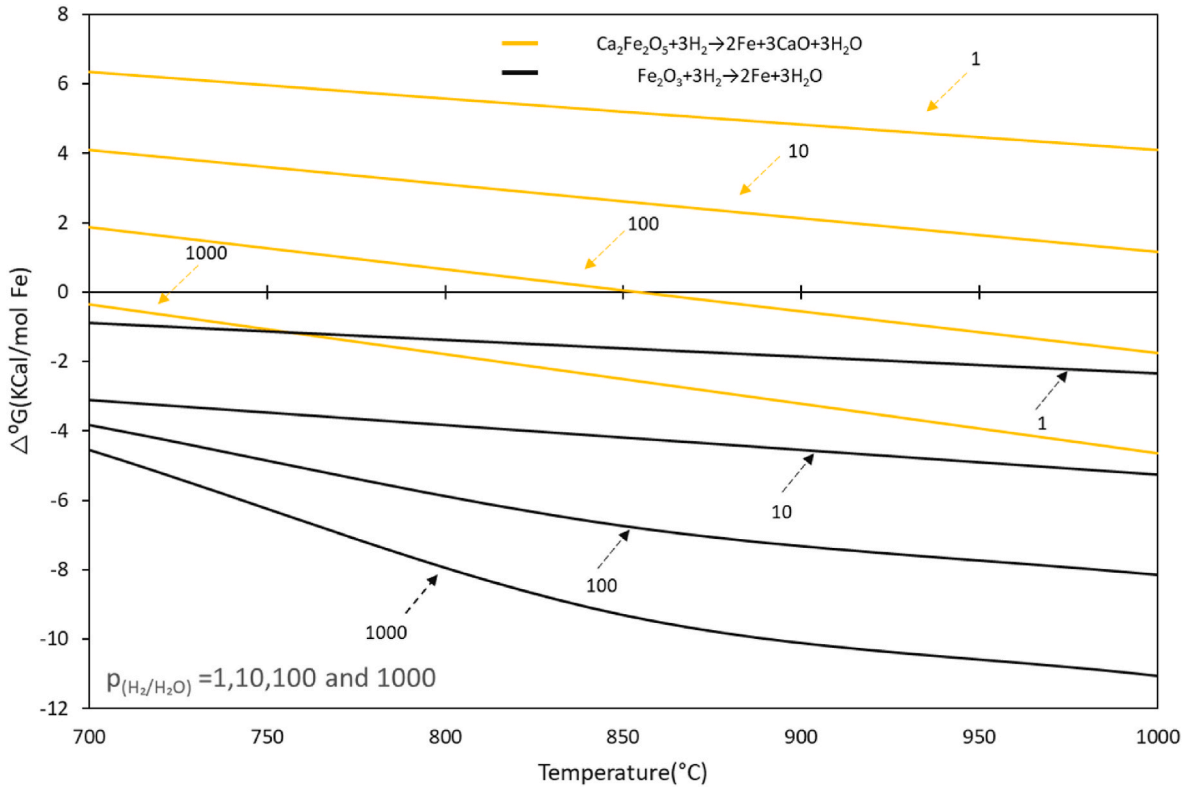

Fig. 9. Free energy for the reduction of brownmillerite to iron at different reduction temperatures, calculated by FactSage version 8.2.

pressure of $H_2/H_2O = 1$.

4. Conclusions

In this work, hydrogen reduction of bauxite residue, bauxite residue-calcium oxide self-hardened, bauxite residue-calcium oxide sintered, and iron ore pellets at different reduction was investigate, the main conclusion are as follows:

- The porosity of pellets made from bauxite residue are high (50–60 vol%), which is significantly greater than that of iron ore pellets (20–30 vol%). The Fe-bearing oxide exists in the form of hematite in iron ore, bauxite residue, and self-hardened CaO-added bauxite residue pellets, whereas it appears as brownmillerite in the bauxite residue CaO-added sintered pellets.
- Although the reduction of Brownmillerite is not feasible at $p_{H_2/H_2O} = 1$ from the thermodynamic point of view (using currently available thermodynamic software), however, it has been observed that the reduction becomes favorable with increasing p_{H_2/H_2O} ratio and elevated applied temperatures.
- The reduction rate of pellets depends on both the porosity and the grain size of iron complexes (brownmillerite and hematite). The higher porosity and smaller hematite particle size in the pellets of bauxite residue, and self-hardened CaO-added bauxite residue yielded higher degree of reduction than the hematite iron ore pellet.
- The rate of brownmillerite reduction is more temperature dependent compared to hematite. It exhibited a slower reduction rate than hematite at 700 °C, while the difference is decreased with increasing temperature to 1000 °C. As the reduction progresses, the reduction mechanism changes from a fast chemically controlled reaction to a slow diffusion-controlled reaction, while an intermediate transition stage exists. The extent and rate of reduction in these stages are significantly influenced by the pellet type utilized and its inherent characteristics.
- The microstructure of reduced pellets, particularly in terms of iron distribution, differs markedly. Fine iron particles are more clustered in bauxite residue, and self-hardened CaO-added bauxite residue pellets compared to sintered CaO-added bauxite residue pellets.

Declaration of competing interest

The authors declare the following financial interests/personal relationships which may be considered as potential competing interests: Manish Kumar kar reports financial support was provided by Norwegian University of Science and Technology. Manish Kumar Kar reports a relationship with Norwegian University of Science and Technology that includes: employment. The authors have no conflict of interest.

Acknowledgments

This project has received funding from the European Union's Horizon 2020 research and innovation program under grant agreement No. 958307. This publication represents only the authors' views, exempting the community from any liability. The HARARE project website is https://h2020harare.eu/

References

[1] Balat M. Potential importance of hydrogen as a future solution to environmental and transportation problems. Int J Hydrogen Energy 2008;33(15):4013–29. https://www.sciencedirect.com/science/article/pii/S0360319908005272.
[2] Li S, Zhang H, Nie J, Dewil R, Baeyens J, Deng Y. The direct reduction of iron ore with hydrogen. Sustainability 2021;13(16):8866. https://www.mdpi.com/2071-1050/13/16/8866.
[3] Ding C, et al. Isothermal reduction of powdery 2CaO· Fe2O3 and CaO· Fe2O3 under H2 atmosphere. Int J Hydrogen Energy 2021;43(1):24–36. https://www.sciencedirect.com/science/article/pii/S0360319917343938.
[4] Metolina P, Ribeiro TR, Guardani R. Hydrogen-based direct reduction of industrial iron ore pellets: statistically designed experiments and computational simulation. Int J Miner Metall Mater 2022;29(10):1908–21. https://link.springer.com/article/10.1007/s12613-022-2487-3.

[5] Szekely J, Evans JW. The effect of grain size porosity and temperature on the reaction of porous pellets. Chem Eng Sci 1971;26:1901–13. https://www.sciencedirect.com/science/article/pii/0009250971860335.
[6] Turkdogan ET, Olsson RG, V Vinters J. Gaseous reduction of iron oxides: Part II. Pore characteristics of iron reduced from hematite in hydrogen. Metall Mater Trans B 1971;2:3189–96. https://www.scirp.org/(S(i43dyn45te-exjx455qlt3d2q))/reference/referencespapers.aspx?referenceid=2137364.
[7] Kawasaki E, Sanscrainte J, Walsh TJ. Kinetics of reduction of iron oxide with carbon monoxide and hydrogen. AIChE J 1962;8(1):48–52. https://aiche.onlinelibrary.wiley.com/doi/abs/10.1002/aic.690080114.
[8] Ma Y, Filho I, Zhang X, nandy S, barriobero-Vila P, Requena G, et al. Hydrogen-based direct reduction of iron oxide at 700° C: heterogeneity at pellet and microstructure scales. Int J Miner Metall Mater 2022;29(10):1901–7. https://link.springer.com/article/10.1007/s12613-022-2440-5.
[9] Spreitzer D, Schenk J. Reduction of iron oxides with hydrogen—a review. Steel Res Int 2019;90(10):1900108. https://onlinelibrary.wiley.com/doi/full/10.1002/srin.201900108.
[10] Kar MK, van der Eijk C, Safarian J. Kinetics study on the hydrogen reduction of bauxite residue-calcite sintered pellets at elevated temperature. Metals 2023;13(4):644. https://www.mdpi.com/2075-4701/13/4/644.
[11] Man Y, Feng J. Effect of gas composition on reduction behavior in red mud and iron ore pellets. Powder Technol 2016;301:674–8. https://www.sciencedirect.com/science/article/pii/S0032591016303515.
[12] Kar MK, Hassanzadeh A, van der Eijk C, Kowalczuk PB, Aasly K, Safarian J. Properties of self-hardened CaO-added bauxite residue pellets, and their behavior in hydrogen reduction followed by leaching and magnetic separation for iron and alumina recovery. Int J Hydrogen Energy 2023;;48(99):38976–90. https://www.sciencedirect.com/science/article/pii/S0360319923048310.
[13] Skibelid OB, Velle SO, Vollan F, Van der Eijk C, Hoseinpur-Kermani A, Safarian J. Isothermal hydrogen reduction of a lime-added bauxite residue agglomerate at elevated temperatures for iron and alumina recovery. Materials 2022;15(17):6012. https://www.mdpi.com/1996-1944/15/17/6012.
[14] Kar MK, Safarian J. Characteristics of bauxite residue–limestone pellets as feedstock for Fe and Al2O3 recovery. Processes 2023;11(1):137. https://www.mdpi.com/2227-9717/11/1/137.
[15] Kar MK, Van Der Eijk C, Safarian J. Hydrogen reduction of high temperature sintered and self-hardened pellets of bauxite residue produced via the addition of limestone and quicklime. In: Proceedings of the 40th international ICSOBA conference, athens, Greece; 2022. p. 11. 10–14 October.
[16] Liang Z, et al. Insight of iron ore-coal composite reduction in a pilot scale rotary kiln: a post-mortem study. Powder Technol 2019;356:691–701. https://www.sciencedirect.com/science/article/pii/S0032591019302876.
[17] Yadav US, Pandey BD, Das BK, Jena DN. Influence of magnesia on sintering characteristics of iron ore. Ironmak Steelmak 2002;29(2):91–5. https://www.tandfonline.com/doi/abs/10.1179/030192302225002018.
[18] Kim S-H, et al. Influence of microstructure and atomic-scale chemistry on the direct reduction of iron ore with hydrogen at 700 C. Acta Mater 2021:116933. 212, https://www.sciencedirect.com/science/article/pii/S135964542100313X.
[19] Lv X, Bai C, Deng Q, Huang X, Qiu G. Behavior of liquid phase formation during iron ores sintering. ISIJ Int 2011;51(5):722–7. https://www.jstage.jst.go.jp/article/isijinternational/51/5/51_5_722/_article.